

1 Brown adipose expansion and remission of glycemic dysfunction in obese SM/J mice  
2

3  
4 Caryn Carson<sup>1</sup>, Juan F Macias-Velasco<sup>1</sup>, Subhadra Gunawardana<sup>2</sup>, Mario A Miranda<sup>1</sup>, Sakura Oyama<sup>1</sup>,  
5 Heather Schmidt<sup>1</sup>, Jessica P Wayhart<sup>1</sup>, Heather A Lawson<sup>1,#</sup>

6  
7  
8  
9  
10 <sup>1</sup>Department of Genetics, Washington University School of Medicine, 660 South Euclid Ave,  
11 Saint Louis, MO, USA

12 <sup>2</sup>Department of Cell Biology and Physiology, Washington University School of Medicine, 660 South Euclid  
13 Ave, Saint Louis, MO, USA

14 <sup>3</sup>Department of Medicine, Washington University School of Medicine, 660 South Euclid Ave, Saint Louis,  
15 MO, USA

16  
17  
18  
19  
20  
21  
22  
23 #Corresponding author  
24 660 South Euclid Ave  
25 Campus Box 8232  
26 Saint Louis, MO, 63110  
27 ph: 314-362-7269, fax: 314-362-7855

28  
29  
30  
31  
32  
33  
34  
35  
36  
37 Keywords: glycemic control, brown adipose, obesity, metabolism, mouse model, transcriptome  
38  
39  
40  
41  
42  
43  
44  
45  
46  
47  
48  
49  
50  
51

52    **Abstract**

53    Disruption of glucose homeostasis increases the risk of type II diabetes, cardiovascular disease, stroke,  
54    and cancer. We leverage a novel rodent model, the SM/J mouse, to understand glycemic control in  
55    obesity. On a high fat diet, obese SM/J mice initially develop impaired glucose tolerance and elevated  
56    fasting glucose. Strikingly, their glycemic dysfunction resolves by 30 weeks of age despite persistence of  
57    obesity. A prominent phenotype is that they dramatically expand their brown adipose depots as they  
58    resolve glycemic dysfunction. This occurs naturally and spontaneously on a high fat diet, with no  
59    temperature or genetic manipulation. When the brown adipose depot is removed from normoglycemic  
60    obese mice, fasting blood glucose and glucose tolerance revert to unhealthy levels, and animals become  
61    insulin resistant. We identified 267 genes whose expression changes in the brown adipose when the  
62    mice resolve their unhealthy glycemic parameters, and find the expanded tissue has a 'healthier'  
63    expression profile of cytokines and extracellular matrix genes. We describe morphological, physiological,  
64    and transcriptomic changes that occur during the unique brown adipose expansion and remission of  
65    glycemic dysfunction in obese SM/J mice. Understanding this phenomenon in mice will open the door for  
66    innovative therapies aimed at improving glycemic control in obesity.

67

68    **Significance Statement**

69    Some obese individuals maintain normal glycemic control. Despite being obese, these individuals  
70    have low risk for metabolic complications, including type-II diabetes. If we better understood why some  
71    obese people maintain normoglycemia then we might develop new approaches for treating metabolic  
72    complications associated with obesity. However, the causative factors underlying glycemic control in  
73    obesity remain unknown. We discovered that, despite persistence of the obese state, SM/J mice enter  
74    into diabetic remission: returning to normoglycemia and reestablishing glucose tolerance and improving  
75    insulin sensitivity. A prominent phenotype is that they dramatically expand their brown adipose depots as  
76    they resolve glycemic dysfunction. Understanding this phenomenon in mice will open the door for  
77    innovative therapies aimed at improving glycemic control in obesity.

78     **Introduction**

79         An estimated 10-30% of obese individuals maintain glycemic control and some longitudinal  
80         studies suggest their risk of developing type II diabetes is no greater than matched lean individuals (1).  
81         No causative factors underlying glycemic control in obesity have been discovered, however the strongest  
82         predictors of impaired glycemic control in obesity are increased visceral fat mass and adipose tissue  
83         dysfunction (2,3). Thus research efforts have focused on understanding the genetic and physiological  
84         mechanisms of action of adipose. Recent research reveals that brown adipose activity is associated with  
85         anti-diabetic properties. Cold exposure in both obese and lean individuals causes increased uptake of  
86         fatty acids and glucose into brown adipose tissue (4). Further, increased brown adipose activity has been  
87         shown to improve glucose homeostasis and insulin sensitivity in adults (5). Transplantation of brown  
88         adipose tissue into mouse models of diabetes greatly improves glucose parameters, including fasting  
89         glucose levels and response to a glucose challenge (6). While there are a variety of obese and diabetic  
90         mouse models, there are no mouse models for understanding the relationship between brown adipose  
91         and glycemic control in obesity.

92         The SM/J inbred mouse strain has long been used for studying interactions between diet and  
93         metabolism, and more recently has started to help uncover the genetic architecture underlying diet  
94         induced obesity and glucose homeostasis. It has previously been shown that fed a high fat diet, SM/J  
95         mice display many of the characteristics of a diabetic-obese mouse: obesity, hyperglycemia and glucose  
96         intolerance at 20 weeks of age (7,8). We discovered that SM/J mice undergo a remarkable transformation  
97         between 20 and 30 weeks of age. Despite persistence of the obese state, these mice enter into diabetic  
98         remission: returning to normoglycemia and reestablishing glucose tolerance and improving insulin  
99         sensitivity. Contemporary with this remission of glycemic parameters is a dramatic expansion of the  
100         intrascapular brown adipose depot. This study describes the morphological, physiological, and  
101         transcriptomic changes that occur during this transition, and establishes the SM/J mouse as a unique  
102         model for understanding the relationship between brown adipose and glycemic control in obesity.

103 Understanding this relationship in a genetic model of glycemic resolution will set the stage for identifying  
104 novel, potentially therapeutic targets for the improvement of glycemic control.

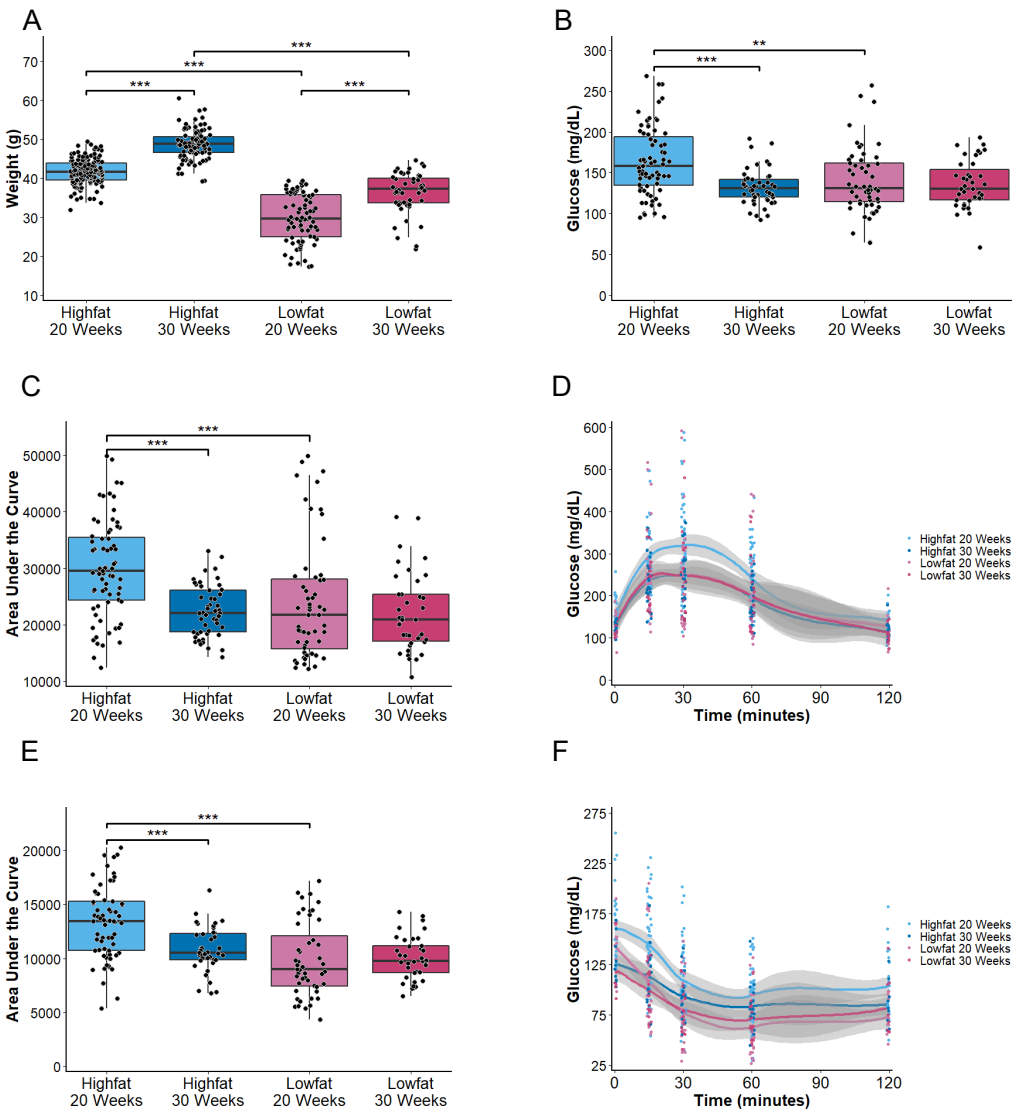
105

106 **Results**

107 *SM/J mice improve glucose parameters without weight loss*

108 When fed a high fat diet (**Supplemental Table 1**) from 3 weeks of age, SM/J mice develop  
109 obesity, hyperglycemia, and impaired glucose tolerance by 20 weeks (9). By 30 weeks, despite the  
110 persistence of obesity, high fat-fed SM/J's resolve their hyperglycemia and impaired glucose tolerance  
111 to levels indistinguishable from low fat-fed controls (**Figure 1A-D**). Further, 30 week old high fat-fed SM/J  
112 mice improve insulin sensitivity (**Figure 1E and F**).

113 High fat-fed C57BL/6J mice also show a reduction in fasting glucose that is accompanied by  
114 increased insulin with age (10). In contrast to SM/J, the difference in circulating glucose between the high  
115 fat- and low fat-fed C57BL/6J remain significantly different over time. Moreover, high fat-fed C57BL/6J  
116 mice show marked glucose intolerance that does not resolve with age. We observe a similar trend in the  
117 LG/J strain of mice, where high fat-fed animals maintain higher fasting glucose levels and impaired  
118 glucose tolerance relative to low fat-fed controls as they age (**Supplemental Figure 1**). The unique  
119 remission of hyperglycemia and improved glucose tolerance observed in the high fat-fed SM/J strain  
120 indicates a genetic basis.



121

122 **Figure 1. Obese SM/J mice improve glucose parameters between 20 and 30 weeks of age. A** High  
123 fat-fed mice weigh significantly more than low fat-fed mice, and SM/J mice gain weight between 20 and  
124 30 weeks of age on both diets, n = 48-131 mice per cohort. **B** 30 week-old high fat-fed mice have  
125 significantly lower fasting glucose levels than at 20 weeks, which is no different than low fat-fed controls,  
126 n = 22-47 mice per cohort. **C and D** 30 week-old high fat-fed mice have improved glucose tolerance  
127 relative to 20 weeks, n = 22-47 mice per cohort. **E and F** Lower fasting glucose and improved glucose  
128 tolerance corresponds with improved insulin sensitivity, n = 22-47 animals per cohort. Equal numbers of  
129 males and females represented; \* p<0.05, \*\* p < 0.01, \*\*\* p < 0.001

130

131

132 *High fat-fed SM/J mice expand their interscapular brown adipose tissue depots*

133

Contemporary with the resolution of glycemic parameters, high fat-fed SM/J mice dramatically

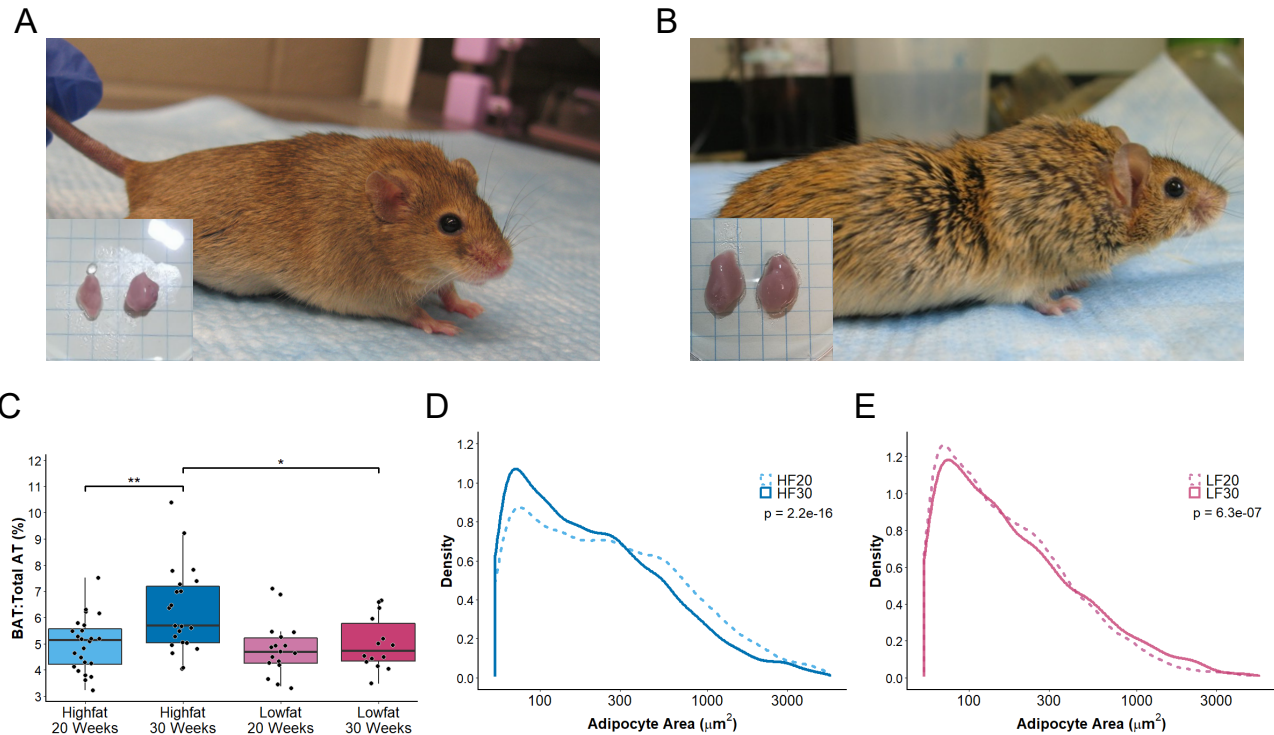
134

expand their intrascapular brown adipose depots, which is not seen in low fat-fed control mice (**Figure**

135 2A-C). This has never been described in another mouse strain, and we do not observe the phenomenon  
136 in the LG/J strain of mice on the same diets at any age (**Supplemental Figure 2**). To understand whether  
137 the tissue mass expansion is due to increased size of individual cells or to increased number of total  
138 cells, we quantified adipocyte cell size and the mitotic index. There are no significant differences in  
139 average cell size in high fat-fed mice between 20 and 30 weeks, or relative to low fat-fed controls  
140 (**Supplemental Figure 3A**). Mice on both diets undergo altered adipocyte area profiles between 20 and  
141 30 weeks of age, however the low fat tissue develops a profile significantly trending towards larger  
142 adipocytes at 30 weeks ( $p=6.4^{-07}$ ) whereas the high fat tissue develops a profile significantly trending  
143 towards smaller adipocytes at 30 weeks ( $p=2.2^{-16}$ ) (**Figure 2D and E**). This suggests that the expansion  
144 of the brown adipose depot in high fat-fed mice is the result of increased proliferation of adipocytes, as  
145 newer adipocytes are smaller due to less lipid accumulation. This is supported by quantification of brown  
146 adipose cells stained positive for the mitotic marker phosphohistone H3, which trends towards a higher  
147 mitotic index in the brown adipose of high fat-fed animals (**Supplemental Figure 3B**).

148 Because obesity has been associated with structural and functional “whitening” of brown adipose  
149 depots in rodents (11–14), we performed experiments to confirm that the tissue expansion in SM/J mice  
150 has the expected properties of brown fat. Histological analysis of the fat depot taken from high fat-fed  
151 SM/J mice at 30 weeks of age confirms the adipocytes in this expansion are brown adipocytes, with small  
152 multilocular lipid droplets and high UCP1 staining (**Supplemental Figure 3C-J**). Expression of canonical  
153 brown adipose genes *Ucp1* and *Cidea* do not change between 20 and 30 weeks (**Supplementary Figure**  
154 **4A-B**). Further, expression of *Tbx1*, a marker specific for beige adipocytes (15), indicates that neither  
155 brown nor white adipose is “beiging” (**Supplementary Figure 4C**). Finally, there is no significant  
156 difference in brown adipose tissue mitochondrial content between the diets or ages (**Supplementary**  
157 **Figure 4D**). There is no difference in core body temperature or circulating free fatty acids between high  
158 and low fat-fed cohorts or between 20 and 30 weeks of age (**Supplemental Figure 5A and B**).  
159 Additionally, while there are diet-dependent differences in the catecholamines norepinephrine and  
160 epinephrine, which activate UCP1-mediated leak respiration and non-shivering thermogenesis, there is

161 no change in levels between ages in the high fat-fed mice (**Supplemental Figure 5C and D**). Thus, the  
162 interscapular adipose depot in high fat-fed SM/J mice maintains a brown adipose identity after expansion  
163 that is not dependent on whole-animal beiging, and is also not associated with altered thermogenesis.



164

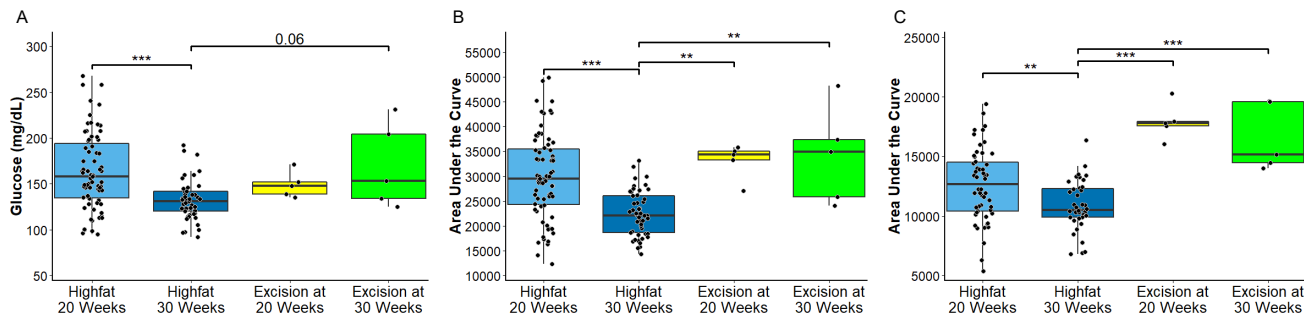
165 **Figure 2. Brown adipose expansion in 30 week-old high fat-fed SM/J mice.** Representative pictures  
166 of **A** 20 week and **B** 30 week-old high fat-fed female mice. **C** Quantification of interscapular brown adipose  
167 depot as a proportion of total fat mass, n = 16-25 mice per cohort. **D** and **E** Cell area density graphs for  
168 high fat and low fat-fed cohorts. Data are plotted on a log10 scale for visualization, n = 4 mice per cohort.  
169

170 *Glucose parameters revert to an unhealthy state in SM/J mice when the brown adipose depot is removed*

171 If the brown adipose expansion is directly related to the glycemic resolution of the high fat-fed  
172 SM/J mice, preventing or removing that expansion should revert the glucose parameters to their  
173 unhealthy state. To test these predictions, we removed the interscapular brown adipose depots from  
174 hyperglycemic 20 and normoglycemic 30 week-old mice. After recovery, at 30 and 35 weeks of age, we  
175 measured basal glucose levels and performed glucose and insulin tolerance tests. We find that  
176 improvement in glucose and insulin tolerance is prevented when the brown adipose depot is removed

177 before expansion. Previously normoglycemic mice revert to unhealthy, 20 week-old measurements when  
178 the brown adipose depot is removed after expansion (**Figure 3 A-C**). These results indicate that the  
179 expanded brown adipose tissue is necessary for the observed remission of glucose intolerance, and for  
180 the maintenance of both glucose tolerance and insulin sensitivity in high fat-fed SM/J mice.

181



182

183 **Figure 3. Glycemic parameters revert to unhealthy levels when the brown adipose depot is**  
184 **removed.** **A** Blood glucose assessed after a 4 hour fast. **B** A glucose tolerance test indicates removal of  
185 the brown adipose depot before (20 week excision) or after (30 week excision) expansion significantly  
186 reduces glucose tolerance. **C** Removal of the brown adipose tissue also significantly increases insulin  
187 resistance. n = 5 excision animals per cohort, representing 4 males and 1 female.

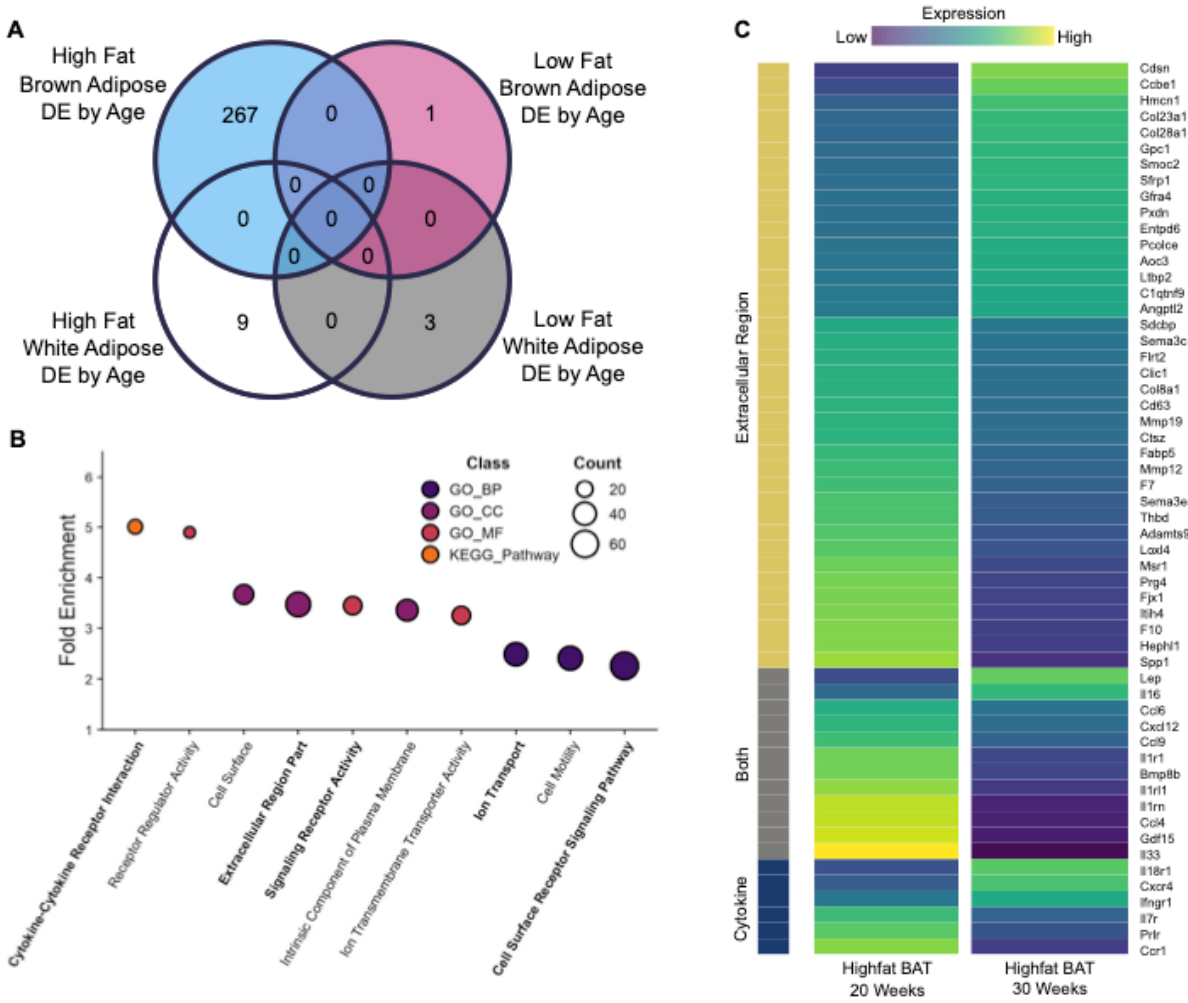
188

189 RNA sequencing reveals enrichment of differentially expressed cytokines and genes affecting extra  
190 cellular matrix

191 Since the brown adipose tissue expansion is unique to high fat-fed SM/J mice, we anticipated that  
192 there would be corresponding unique transcriptomic changes in the brown adipose. Indeed, we identified  
193 267 genes whose expression significantly and uniquely changes between 20 and 30 weeks of age in  
194 high fat-fed SM/J brown adipose tissue (at a 5% FDR, out of 13,253 total genes expressed;  
195 **Supplemental Table 2**). These expression changes occur when the mice resolve their glycemic  
196 dysfunction and expand their brown adipose depots. These genes are not differentially expressed in  
197 white adipose tissue taken from the same animals or in low fat-fed SM/J controls (**Figure 4A**).  
198 Additionally, they are not differentially expressed in the LG/J strain of mouse, once again underscoring  
199 the genetic basis of the phenomenon (**Supplemental Table 3**).

200 Over-representation analysis indicates these genes are enriched for those involved in cytokine-  
201 cytokine receptor interactions ( $p=3.23e^{-06}$ ), signaling receptor activity ( $p = 5.70e^{-06}$ ), cell surface receptor  
202 signaling ( $p=2.04e^{-07}$ ), and extracellular matrix components ( $p = 7.93 e^{-13}$ ) (**Figure 4B**). These are  
203 intriguing results because brown adipose has been identified as a source of cytokines that influence  
204 glucose homeostasis, and extracellular matrix changes are essential for tissue expansion, cellular  
205 signaling, and regulation of growth factor bioavailability.

206 Several genes belonging to these biological categories have evidence for their involvement in  
207 glucose homeostasis and change expression in a direction that is associated with improved metabolic  
208 health in high fat-fed SM/J mice between 20 and 30 weeks of age (**Figure 4C; Supplemental Table 2**).  
209 In particular, the direction of expression change reveals that the expansion of brown adipose is  
210 associated with decreased expression of inflammatory (e.g. interleukin 7 receptor, *Il7r*) (16) and fibrotic  
211 markers (e.g. collagen type VIII alpha 1 chain, *Col8a1*; semaphorin 3C, *Sema3c*) (17,18), and changes  
212 in extracellular matrix components (e.g. matrix metallopeptidase 12, *Mmp12*; procollagen c-  
213 endopeptidase enhancer, *Pcolce*) (19,20) and cytokines (e.g. coagulation factor VII, *F7*; leptin, *Lep*;  
214 secreted frizzled-related protein 1, *Sfrp1*) (21–23). These genes are not differentially expressed in white  
215 adipose from the same animals, and they are not differentially expressed in low fat-fed brown or white  
216 adipose between 20 and 30 weeks (**Supplemental Figure 6**). Other mouse models of diet-induced  
217 obesity develop unhealthy brown adipose transcriptomes characterized by increased expression of pro-  
218 inflammatory genes and fibrotic markers (24). The direction of expression change in our brown adipose  
219 tissue supports the uniqueness of the high fat-fed SM/J mice.



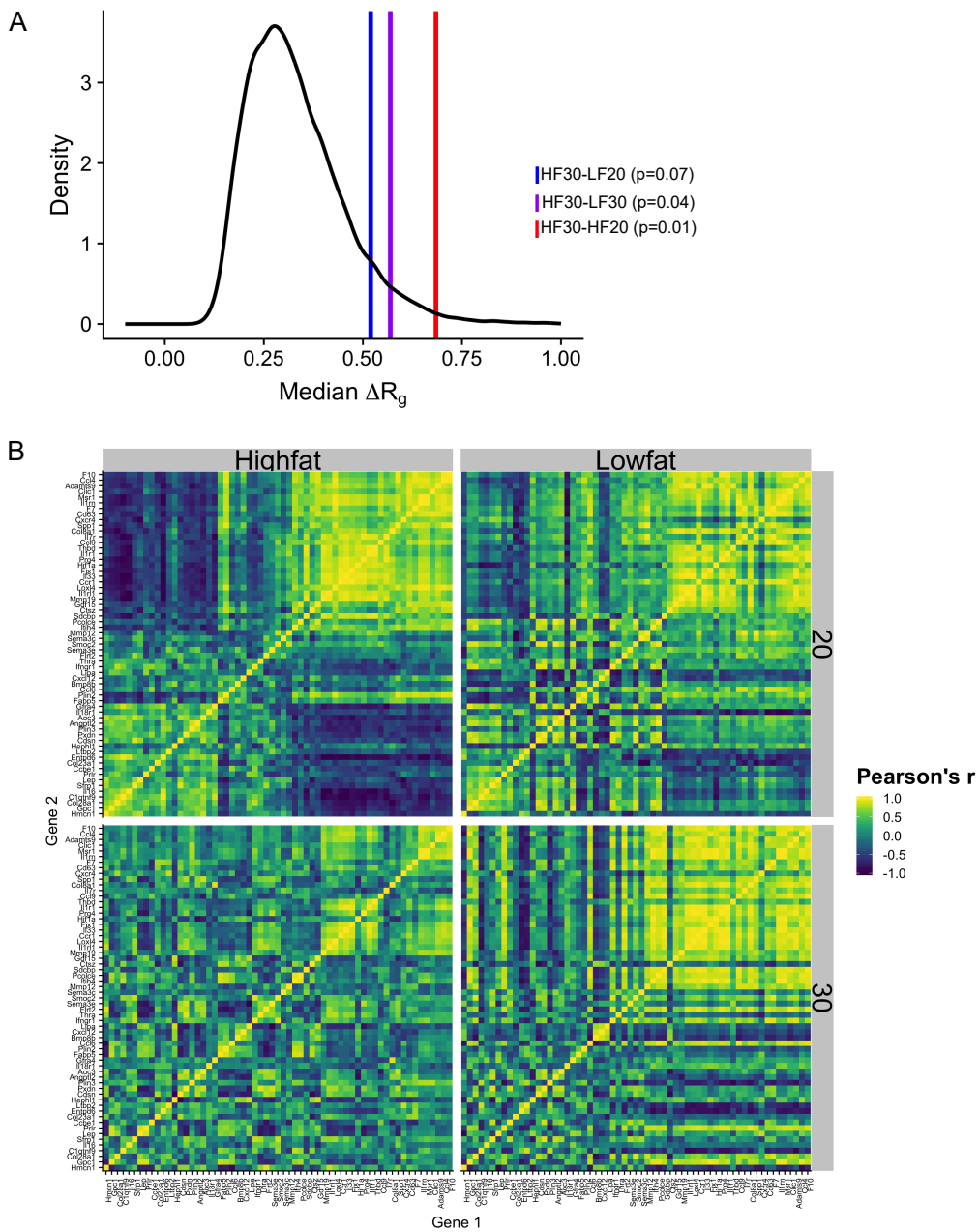
221

222 **Figure 4. High fat-fed SM/J mice have unique brown adipose differential expression between 20**  
 223 **and 30 weeks of age. A Venn diagram illustrating the number of genes differentially expressed between**  
 224 **high and low fat-fed 20 and 30 week-old SM/J interscapular brown or reproductive white adipose tissues.**  
 225 **No genes are differentially expressed in more than one diet-by-tissue cohort. B Enriched terms colored**  
 226 **by class (Gene Ontology Biological Process (GO\_BP), Cellular Component (GO\_CC), Molecular**  
 227 **Function (GO\_MF), and KEGG Pathway. C Heatmap of differentially expressed brown adipose tissue**  
 228 **genes between high fat-fed 20 and 30 week-old mice belonging to cytokine, extracellular matrix, or both**  
 229 **gene ontologies. Equal numbers of males and females represented, n = 8 animals per age-by-diet cohort.**

230 30 week old high fat-fed SM/J brown adipose has a healthier co-expression profile

231 Because variation in glucose homeostasis is complex and the result of many interacting genes,  
 232 we examined the co-expression profile of genes belonging to the enriched cytokine and extracellular  
 233 matrix (ECM) biological categories (**Figure 4B and C**). We find that the co-expression profile of the  
 234 differentially expressed ECM and cytokine genes is significantly different between 20 and 30 week-old

235 high fat-fed animals ( $p=0.01$ ). To determine if the co-expression profile of these genes in 30 week-old  
236 high fat-fed animals' brown adipose is more similar to the 20 week-old high fat-fed or to the low fat-fed  
237 animals', we compared the overall co-expression correlation structure between the diet and age cohorts  
238 for these genes. Remarkably, we find the 30 week-old high fat-fed SM/J brown adipose ECM and cytokine  
239 co-expression profile is most similar to the 20 week-old low fat-fed animals' (probability of difference  
240 between high fat-fed 30 weeks and low fat-fed 20 weeks = 0.07; probability of difference between high  
241 fat-fed 30 weeks and low fat-fed 30 weeks = 0.04) (**Figure 5A**). Thus, the brown adipose cytokine and  
242 ECM gene co-expression profile appears 'healthier' in 30 week-old high fat-fed animals after expansion  
243 and remission of the diabetic phenotype. This is illustrated in **Figure 5B**.



244

245 **Figure 5. High fat-fed 30 week-old SM/J mice have a cytokine and ECM gene co-expression profile**  
 246 **most similar to low fat-fed 20 week-old mice.** A The median change in correlation structure is plotted  
 247 as a vertical line against the null model. High fat-fed 30 week-old SM/J mice have a co-expression profile  
 248 significantly different from high fat-fed 20 week-old SM/J mice, and not significantly different from low fat-  
 249 fed 20 week-old mice. B Heatmap of the gene expression correlation matrices for each cohort. HF30 =  
 250 high fat-fed 30 week-old; HF20 = high fat-fed 20 week-old; LF30 = low fat-fed 30 week-old; LF20 = low  
 251 fat-fed 20 week-old. Equal numbers of males and females represented, n = 8 animals per age-by-diet  
 252 cohort.  
 253

254     **Discussion**

255         Obesity (body-mass index [BMI]  $\geq 30 \text{ kg.m}^2$ ) is associated with serious metabolic complications,  
256         including type II diabetes, cardiovascular disease, cancer, and stroke (25–29). Currently, 38% of  
257         American adults are classified as obese, 9.4% have type II diabetes, and an additional 34% are pre-  
258         diabetic, costing 327 billion dollars in annual medical costs (30,31). Obesity and diabetes are tightly  
259         linked; obesity raises the risk of developing type II diabetes 27–76 fold, while approximately 60% of  
260         diabetics are obese (25,30,32,33). Though weight loss is *the* gold standard for treating glycemic  
261         dysfunction in obesity, many obese people are unable to achieve long-term weight loss (34,35). Currently,  
262         metformin and thiazolidinediones are prescribed to prevent the development of diabetes in obese  
263         individuals, but pharmacological therapy has been shown to have only modest protective effects (33,36).  
264         Greater understanding of the relationship between obesity and glycemic control is needed to develop  
265         more effective preventative measures for obese patients.

266         Here we describe morphological, physiological, and transcriptomic changes that occur during  
267         brown adipose expansion and remission of glycemic dysfunction in obese SM/J mice. The SM/J strain  
268         was derived from a pool of seven inbred strains and selected for small body size at 60 days (37). The  
269         strain has been used extensively in genetic studies of complex traits related to growth and metabolism,  
270         particularly because SM/J mice are strongly responsive to high fat diet-induced obesity. These studies  
271         all used mice aged 20 weeks or less, when SM/J mice develop the classic hallmarks of obese-diabetic  
272         mice. We discovered that by 30 weeks of age, contemporary with a dramatic expansion of intrascapular  
273         brown adipose tissue, their hyperglycemia and impaired glucose tolerance go into remission despite  
274         persistence of obesity. Dissecting the genetic basis of this phenomenon has the potential to uncover  
275         novel relationships among brown adipose, glucose homeostasis, and obesity.

276         We identified 267 genes whose expression significantly and uniquely changes between 20 and  
277         30 weeks of age in high fat-fed SM/J brown adipose tissue (**Figure 5A**). We focus on genes associated  
278         with ECM and cytokine activity because both biological categories are enriched in the set of genes that  
279         significantly change expression in brown adipose during the remission of glycemic parameters. Brown

280 adipose is a source of endocrine signals with anti-diabetic properties and is involved in extensive cross-  
281 talk with other organs (38). It secretes cytokines that influence whole-body glucose homeostasis and  
282 insulin sensitivity including IGF1, FGF21, NRG-3 and NRG-4 (39). ECM changes are essential for cellular  
283 signaling, regulation of growth factor bioavailability, and accompany healthy adipose expansion.  
284 However, extreme changes in ECM protein levels are associated with adipose dysfunction in obesity;  
285 thus a fine balance between tissue remodeling and excessive accumulation of ECM proteins must be  
286 achieved to maintain adipose tissue homeostasis (18).

287 We highlight 8 cytokines and ECM genes that significantly change expression in a direction  
288 associated with improved metabolic health in previous studies. *Il7r*, which was found to be one of the  
289 highest ranking genes in the white adipose tissue inflammatory response pathway (40), decreases  
290 expression between 20 and 30 weeks of age in high fat-fed SM/J brown adipose. *Col8a1* and *Sema3C*  
291 are both associated with adipose tissue fibrosis (17,41). Increased adipose tissue fibrosis is a signature  
292 of dysfunctional adipose and is associated with impaired glucose homeostasis and insulin resistance  
293 (18). Both *Col8a1* and *Sema3c* expression decrease between 20 and 30 weeks in high fat-fed SM/J  
294 brown adipose. *Mmp12* is an enzyme that contributes to adipose tissue remodeling (42). Increased  
295 *Mmp12* expression is associated with white adipose tissue inflammation and insulin resistance and  
296 *Mmp12*<sup>-/-</sup> mice are more insulin sensitive than wildtype controls on a high fat diet (19). Its expression  
297 decreases in 30 week old high fat-fed SM/J brown adipose. *Pcolce* encodes a glycoprotein that regulates  
298 collagen processing at the ECM (43). Mice with defects in ECM collagen are glucose intolerant,  
299 hyperglycemic, and insulin resistant (20). PCOLCE is one of 15 key drivers that collectively account for  
300 22% of GWAS hits for type II diabetes in a recent multiethnic meta-analysis (44). *Pcolce* expression is  
301 significantly increased in 30 week old high fat-fed SM/J brown adipose. *F7*, *Lep*, and *Sfrp1* are each  
302 secreted proteins. Increased *F7* plays a role in the pathogenesis of obesity (45). In particular it has been  
303 shown to induce beta cell death and impaired islet glucose-stimulated insulin secretion (21). Increased  
304 *Lep* can dramatically lower blood glucose levels in diabetic rodent models (23). In brown adipose, leptin  
305 has been shown to stimulate glucose uptake (46). *Sfrp1* is dysregulated in obesity and *Sfrp1*<sup>-/-</sup> mice have

306 elevated blood glucose and impaired glucose tolerance when fed a high fat diet (22). *F7* expression is  
307 decreased and *Lep* and *Sfrp1* are increased in 30 week old high fat-fed SM/J brown adipose tissue. Most  
308 of what is known about the role of these 8 genes in adipose comes from studies of white adipose tissue,  
309 but none of these genes are differentially expressed in SM/J white adipose. Many additional genes likely  
310 contribute to the observed phenomenon, however little, if anything, is known about their role in brown  
311 adipose tissue. The 267 differentially expressed genes we identified represent a set of actionable  
312 candidates for further functional studies of their role in brown adipose and glucose homeostasis.

313 There is great interest in harnessing the potential of brown adipose to treat obesity and diabetes,  
314 either through the calorie burning action of non-shivering thermogenesis or the endocrine action of  
315 adipokines. Research into the effects of brown adipose on systemic metabolism is in its infancy, and the  
316 community needs appropriate animal models to interrogate its physiological roles and identify potentially  
317 druggable targets. We present the SM/J mouse strain as a unique model to address this need. The SM/J  
318 mouse provides a tractable, genetic system in which to understand the relationship between brown  
319 adipose and glycemic control in obesity. Understanding this relationship in the SM/J mouse will open  
320 doors for identifying novel, potentially druggable targets for the improvement of glycemic control in  
321 humans.

322

### 323 **Methods**

#### 324 *Animal Husbandry and Phenotyping*

325 SM/J (RRID:IMSR\_JAX:000687) and LG/J (RRID:IMSR\_JAX:000675) mice were obtained from  
326 The Jackson Laboratory (Bar Harbor, ME). Experimental animals were generated at the Washington  
327 University School of Medicine and all experiments were approved by the Institutional Animal Care and  
328 Use Committee in accordance with the National Institutes of Health guidelines for the care and use of  
329 laboratory animals. Pups were weaned at 3 weeks and reared in same-sex cages of 3-5 animals until  
330 necropsy. At weaning, mice were randomly placed on a high fat diet (42% kcal from fat; Teklad  
331 TD88137) or an isocaloric low fat diet (15% kcal from fat; Research Diets D12284) (**Supplemental**

332     **Table 1).** Feeding was *ad libitum*. The animal facility operates on a 12 hour light/dark cycle with a  
333     constant ambient temperature of 21°C. Animals were weighed weekly until sacrifice. At 18 and 28  
334     weeks of age, animals were subject to an intraperitoneal glucose tolerance test after a 4 hour fast. At  
335     19 and 29 weeks of age animals were subject to an intraperitoneal insulin tolerance test. At 20 or 30  
336     weeks of age, body composition was determined by MRI and temperature was measured with a rectal  
337     thermometer. After a 4 hour fast, at 20 or 30 weeks of age, animals were given an overdose of sodium  
338     pentobarbital and blood was collected via cardiac puncture. Euthanasia was achieved by cardiac  
339     perfusion with phosphate-buffered saline. After cardiac perfusion, tissues were collected and flash  
340     frozen in liquid nitrogen and stored at -80°C, or processed according to protocols for histology and  
341     other assays.

342

343     *Blood plasma assays*

344         Fasting blood glucose was measured using a GLUCOCARD Vital glucometer (Arkay, MN USA).  
345         ELISAs measuring plasma levels of free fatty acids (Wako Life Sciences 995-34693) were quantified  
346         according to manufacturer's protocol. Catecholamines were assayed through the Vanderbilt University  
347         Medical Center's Hormone Assay and Analytical Services Core ([www.vumc.org/hormone/assays](http://www.vumc.org/hormone/assays); NIH  
348         grants DK059637 (MMPC) and DK020593 (DRTC)).

349

350     *Brown adipose histology*

351         At the time of tissue collection, small portions of interscapular brown and reproductive white  
352         adipose tissues were placed in 1 mL of neutral buffered formalin. These samples were incubated at 4C  
353         while gently shaking for 24 hours. Immediately afterwards, samples were placed into plastic cages and  
354         processed into paraffin blocks using a Leica tissue processor with the following protocol: 70% EtOH for  
355         1 hour x 2, 85% EtOH for 1 hour, 95% EtOH for 1 hour x 2, 100% EtOH for 1 hour x 2, Xylenes for 1 hour  
356         x 2, paraffin wax. Adipose blocks were sectioned into 6 µm sections, with 2-4 slices on each slide.

357

358 *H&E Staining*

359 Slides were incubated at 60C for 1 hour, then placed in xylenes to remove remaining paraffin wax.  
360 Slides were then rehydrated using successive decreasing EtOH concentrations (xylenes x 2, 100% EtOH  
361 x 2, 95% EtOH, 70% EtOH, H<sub>2</sub>O). Slides were incubated in hematoxylin (Leica Surgipath 3801570),  
362 Define (3803590), Blue Buffer 8 (3802915), and eosin (3801616), and dehydrated (95% EtOH, 100%  
363 EtOH, xylene x 2). Imaging was performed using the Zeiss AxioPlan2 microscope and Olympus DP  
364 software. Analysis of adipocyte size was performed using ImageJ. Images were converted to black and  
365 white and skeletonized to reveal only the cell wall outlines. Cell area was calculated from outlines with a  
366 lower limit of 50 um and upper limit of 700 um to reduce noise. All cells from a cohort (4-7 images each  
367 from 4 animals per cohort, equal numbers of males and females) were pooled for cell area density  
368 analysis. A Welch's unequal variances t-test was performed between ages in each diet to determine  
369 significant differences.

370

371 *Immunofluorescence*

372 Slides were incubated at 60C for 1 hour, then placed in xylenes to remove remaining paraffin wax.  
373 Slides were then rehydrated using successive decreasing EtOH concentrations (xylenes x 2, 50% EtOH  
374 in xylenes, 100% EtOH x 2, 95% EtOH, 70% EtOH, 50% EtOH, 0.3% H<sub>2</sub>O<sub>2</sub> in MeOH, H<sub>2</sub>O). Slides were  
375 washed with TBS and blocked in 10% normal donkey serum (Abcam ab7475) for 1 hour, followed by  
376 incubation with primary antibody overnight at 4C. [Primary antibodies: rabbit anti-Ucp1 (1:100, Sigma  
377 U6382) and mouse anti-PHH3 (1:100, Invitrogen MA5-15220)]. After an additional wash, secondary  
378 antibody was applied for 1 hour at room temperature [Secondary antibodies: donkey anti-rabbit 488  
379 (1:1000, Abcam ab150061) and donkey anti-mouse 647 (1:200, Abcam ab150107)]. Fluoroshield  
380 Mounting Medium with DAPI (Abcam) was applied to seal the coverslip and slides were stored at 4C.

381 Imaging was performed using the Zeiss Confocal microscope and Zen Lite imaging program. PHH3  
382 analysis was performed using the CellProfiler program. Background was subtracted from DAPI and PHH3  
383 channels using ImageJ. DAPI channel was used to identify total nuclei in CellProfiler. Adipose nuclei  
384 images were overlaid with PHH3 stain to identify mitotic adipose nuclei. Mitotic nuclei were summed  
385 across all 4 slides for each individual. Mitotic adipose index is reported as mitotic adipose nuclei divided  
386 by adipose nuclei multiplied by 100%.

387

388 *Quantitative rt-PCR*

389 Total RNA was extracted from brown, subcutaneous inguinal, and visceral reproductive adipose  
390 samples using the Qiagen RNeasy Lipid Kit. High-Capacity cDNA Reverse Transcription Kit  
391 (Thermofisher) was used for reverse transcription. Quantitative-rtPCR was performed to assess  
392 expression levels of target genes with an Applied Biosystems (USA) QuantStudio 6 Flex instrument using  
393 SYBR Green reagent. Results were normalized to *L32* expression, which was experimentally determined  
394 to not be differentially expressed across diet and age cohorts. cDNA products were analyzed using the

395  $\Delta C_T$  method. Primers used: *L32* forward TCCACAATGTCAAGGAGCTG, reverse  
396 GGGATTGGTGAECTCTGATGG; *Cidea* forward TGCTCTCTGTATGCCAGT, reverse  
397 GCCGTGTTAAGGAATCTGCTG; *Tbx1* forward GGCAGGCAGACGAATGTTC, reverse  
398 TTGTCATCTACGGGCACAAAG; *Ucp1* forward CCTCTCCAGTGGATGTGGTAA, reverse  
399 AGAACGCCACAAACCCTTGA.

400

401 *Mitochondrial DNA quantification*

402 DNA was extracted from brown and inguinal adipose tissues using the Qiagen DNeasy Blood and  
403 Tissue Kit. Briefly, 40mg of tissue was homogenized in 10% proteinase K through vortexing and  
404 incubation at 56°C. DNA was precipitated with ethanol, collected in a spin column, and eluted in 150mL  
405 of buffer. DNA concentration was quantified on a Nanodrop, and 50ng was used in a qPCR reaction to

406 quantify the amount of *h19* (nuclear gene) and *CytB* (mitochondrial gene). Mitochondrial content was  
407 calculated as the ratio of mtDNA to nucDNA. Primers used: *Cytb* forward  
408 TCTACGCTCAATCCCCAATAAAC, reverse TTAGGCTTCGTTGCTTGAGGT; *h19* forward  
409 TATGTGCCATTCTGCTGCGA, reverse AAGGTTAGAGAGGGGGCCT.

410

411 *RNA sequencing and analyses*

412 Sixty-four LG/J and SM/J mice were used for sequencing analysis, representing 4 males and 4  
413 females from each diet (high and low fat) and age (20 and 30 weeks). Total RNA was isolated from  
414 interscapular brown and reproductive white adipose tissues using the RNeasy Lipid Tissue Kit (QIAgen).  
415 RNA concentration was measured via Nanodrop and RNA quality/integrity was assessed with a  
416 BioAnalyzer (Agilent). RNAseq libraries were constructed using the RiboZero kit (Illumina) from total RNA  
417 samples with RIN scores >7.5. Libraries were checked for quality and concentration using the DNA  
418 1000LabChip assay (Agilent) and quantitative PCR, according to manufacturer's protocol. Libraries were  
419 sequenced at 2x100 paired end reads on an Illumina HiSeq 4000. After sequencing, reads were de-  
420 multiplexed and assigned to individual samples.

421 FASTQ files were filtered to remove low quality reads and aligned against LG/J and SM/J custom  
422 genomes using STAR (47,48). Briefly, LG/J and SM/J indels and SNVs were leveraged to construct  
423 strain-specific genomes using the GRC38.72-mm10 reference as a template. This was done by replacing  
424 reference bases with alternative LG/J and SM/J bases using custom python scripts. Ensembl R72  
425 annotations were adjusted for indel-induced indexing differences for both genomes. Read counts were  
426 normalized via upper quartile normalization and a minimum normalized read depth of 10 was required.  
427 Alignment summaries are provided in **Supplemental Figure 7**. Library complexity was assessed and  
428 differential expression between each age cohort for each strain-by-diet comparison was determined after  
429 TMM normalization in edgeR (49).

430 Functional enrichment of differentially expressed genes was tested by over-representation  
431 analysis in the WEB-based Gene Set Analysis Toolkit v2019 (50). We performed analyses of gene

432 ontologies (biological process, cellular component, molecular function), pathway (KEGG), and phenotype  
433 (Mammalian Phenotype Ontology). For each tissue, the list of all unique differentially expressed genes  
434 was analyzed against the background of all unique genes expressed in that tissue (Supplemental Tables  
435 2 and 3). A Benjamini-Hochberg FDR-corrected p-value  $\leq 0.05$  was considered significant.

436

437 *Correlation structure*

438 Co-expression was assessed for the set of 62 differentially expressed cytokines and ECM genes  
439 by correlating expression of each gene with the expression of the other 61 genes in each diet-by-age  
440 cohort. Each pair of genes then had their correlations correlated ( $R_g$ ), where gene = G.

441 
$$R_{g,G \in (i,j)} = \text{cor} \left( \begin{bmatrix} \text{cor}(G_i, G_1) \\ \vdots \\ \text{cor}(G_i, G_n) \end{bmatrix}, \begin{bmatrix} \text{cor}(G_j, G_1) \\ \vdots \\ \text{cor}(G_j, G_n) \end{bmatrix} \right)$$

442

443 Gene-pair-correlations were then compared between the high fat-fed 30 week-old cohort and the other  
444 three cohorts (high fat-fed 30 weeks to high fat-fed 20 weeks, high fat-fed 30 weeks to low fat-fed 30  
445 weeks, high fat-fed 30 weeks to low fat-fed 20 weeks) to obtain the  $\Delta R_g$  between a pair of cohorts, where  
446 cohort = K.

447 
$$\Delta R_{g,G \in (i,j), K_1, K_2} = |R_{g,G \in (i,j), K_1} - R_{g,G \in (i,j), K_2}|$$

448

449 The median change in correlation ( $M\Delta R_g$ ) was calculated and permutation was employed to identify the  
450 background of expected  $M\Delta R_g$  values. Permutation was performed by randomly selecting 2 groups of 8  
451 animals from any cohort 10,000 times.

452 
$$M\Delta R_{g,K_1, K_2} = \text{median}(\Delta R_{g,G \in (i,j), K_1, K_2})$$

453

454  $M\Delta R_g$  was determined for the 2 randomized groups ( $rK_1, rK_2$ ) for all 10,000 permutations to generate a  
455 null model. Log transformation was performed to approximate normality, which was determined by Wilks-

456 Shapiro test and Q-Q plot. Significance was drawn from the cumulative normal null model to test if the  
457 difference in correlation structure between each pair of cohorts was greater than by chance under the  
458 randomized null model.

459

$$p_{K_1, K_2} = P(X \geq M\Delta R_{g, K_1, K_2}) \sim \mathcal{N}(\mu_r, \sigma_r)$$

460

461 *Brown adipose excision*

462 Interscapular brown adipose tissue depots were removed from 20 or 30 week-old high fat-fed  
463 SM/J mice. A small longitudinal incision was made between the shoulder blades. All interscapular  
464 adipose tissue was carefully removed, and a cauterizing wand used to stop excessive bleeding when  
465 necessary. Surgeries were performed under general anesthesia by IP injection of ketamine/ xylazine  
466 (100/200 mg/Kg) and mice were maintained in the surgical plane by isofluorane/oxygen for the duration  
467 of the procedure. Incisions were closed with 5-0 nonabsorbable sutures. Ketoprofen (2-5 mg/Kg) was  
468 provided post-procedure and topical antibiotic was applied to the incision for up to 3 days as necessary.  
469 Animal health and well-being was monitored daily. Sutures were removed at 10 days post-surgery. Mice  
470 were allowed to recover for four weeks after surgery or until they reached 30 weeks of age, then  
471 underwent a glucose tolerance test and an insulin tolerance test one week later. After an additional week  
472 of recovery, animals were sacrificed and plasma and multiple tissues harvested (reproductive and  
473 inguinal adipose depots, liver, heart, soleus, pancreas, hypothalamus) as described above.

474

475 *Statistics*

476 Data within individual cohorts were assessed for normality using a Wilks-Shapiro test. Outliers  
477 were identified by a Grubbs test ( $p < 0.05$ ) and removed. Data were tested for significant differences  
478 among cohorts by ANOVA with a Tukey's post-hoc correction. The sex X diet X age term was not  
479 significant for any phenotype so males and females were pooled for analyses. P-values  $<0.05$  were  
480 considered significant. All statistical analyses were performed using the R software package.

481

482 **Acknowledgments**

483 *Author Contributions*

484 HAL and CC designed the experiments. CC, HS, JPW, and HAL performed physiological and molecular  
485 assays. CC, MAM and SO performed histological assays and analyses. CC and SG performed excision  
486 surgeries. CC, JFM and HAL analyzed the RNAseq data. CC and HAL wrote the manuscript. All authors  
487 edited and approved the final draft.

488

489 *Funding*

490 This work was supported by the Washington University Department of Genetics, the Diabetes Research  
491 Center at Washington University (P30DK020579), the NIH NIDDK (K01 DK095003) to HAL and NIH  
492 NIGM (T32 GM007067) to CC.

493

494 The authors declare no conflicts of interest.

495

496 **References**

- 497 1. Meigs JB, Wilson PWF, Fox CS, Vasan RS, Nathan DM, Sullivan LM, et al. Body mass index,  
498 metabolic syndrome, and risk of type 2 diabetes or cardiovascular disease. *J Clin Endocrinol  
499 Metab* [Internet]. 2006 Aug [cited 2016 Aug 31];91(8):2906–12. Available from:  
500 <http://www.ncbi.nlm.nih.gov/pubmed/16735483>
- 501 2. Klöting N, Fasshauer M, Dietrich A, Kovacs P, Schön MR, Kern M, et al. Insulin-sensitive  
502 obesity. *Am J Physiol Metab*. 2010;
- 503 3. Goossens GH. The Metabolic Phenotype in Obesity: Fat Mass, Body Fat Distribution, and  
504 Adipose Tissue Function. *Obes Facts*. 2017;
- 505 4. Saito M, Okamatsu-Ogura Y, Matsushita M, Watanabe K, Yoneshiro T, Nio-Kobayashi J, et al.  
506 High incidence of metabolically active brown adipose tissue in healthy adult humans: Effects of  
507 cold exposure and adiposity. *Diabetes*. 2009;

- 508 5. Chondronikola M, Volpi E, Børshøj E, Porter C, Annamalai P, Enerbæk S, et al. Brown adipose  
509 tissue improves whole-body glucose homeostasis and insulin sensitivity in humans. *Diabetes*.  
510 2014;
- 511 6. Gunawardana SC, Piston DW. Reversal of type 1 diabetes in mice by brown adipose tissue  
512 transplant. *Diabetes*. 2012;
- 513 7. Lawson H a, Zelle KM, Fawcett GL, Wang B, Pletscher LS, Maxwell TJ, et al. Genetic,  
514 epigenetic, and gene-by-diet interaction effects underlie variation in serum lipids in a LG/JxSM/J  
515 murine model. *J Lipid Res*. 2010;
- 516 8. Lawson HA, Lee A, Fawcett GL, Wang B, Pletscher LS, Maxwell TJ, et al. The importance of  
517 context to the genetic architecture of diabetes-related traits is revealed in a genome-wide scan of  
518 a LG/J × SM/J murine model. *Mamm Genome* [Internet]. 2011 Apr [cited 2016 Jan 20];22(3–  
519 4):197–208. Available from:  
520 <http://www.ncbi.nlm.nih.gov/pmc/articles/PMC3650899/>&tool=pmcentrez&rendertype  
521 =abstract
- 522 9. Ehrlich TH, Kenney JP, Vaughn TT, Pletscher LS, Cheverud JM. Diet, obesity, and  
523 hyperglycemia in LG/J and SM/J mice. *Obes Res*. 2003;
- 524 10. Ahren W and. The High-Fat Diet–Fed Mouse. *Diabetes*. 2004;
- 525 11. Shimizu I, Aprahamian T, Kikuchi R, Shimizu A, Papanicolaou KN, MacLauchlan S, et al.  
526 Vascular rarefaction mediates whitening of brown fat in obesity. *J Clin Invest*. 2014;
- 527 12. Shimizu I, Walsh K. The Whitening of Brown Fat and Its Implications for Weight Management in  
528 Obesity. *Current obesity reports*. 2015.
- 529 13. Roberts-Toler C, O'Neill BT, Cypress AM. Diet-induced obesity causes insulin resistance in  
530 mouse brown adipose tissue. *Obesity*. 2015;
- 531 14. Lapa C, Arias-Loza P, Hayakawa N, Wakabayashi H, Werner RA, Chen X, et al. Whitening and  
532 Impaired Glucose Utilization of Brown Adipose Tissue in a Rat Model of Type 2 Diabetes  
533 Mellitus. *Sci Rep*. 2017;

- 534 15. Wu J, Boström P, Sparks LM, Ye L, Choi JH, Giang AH, et al. Beige adipocytes are a distinct  
535 type of thermogenic fat cell in mouse and human. *Cell*. 2012;
- 536 16. Kim D, Kim J, Yoon JH, Ghim J, Yea K, Song P, et al. CXCL12 secreted from adipose tissue  
537 recruits macrophages and induces insulin resistance in mice. *Diabetologia*. 2014;
- 538 17. Mejhert N, Wilfling F, Esteve D, Galitzky J, Pellegrinelli V, Kolditz CI, et al. Semaphorin 3C is a  
539 novel adipokine linked to extracellular matrix composition. *Diabetologia*. 2013;
- 540 18. Sun K, Tordjman J, Clément K, Scherer PE. Fibrosis and adipose tissue dysfunction. *Cell  
541 Metabolism*. 2013.
- 542 19. Lee JT, Pamir N, Liu NC, Kirk EA, Averill MM, Becker L, et al. Macrophage metalloelastase  
543 (MMP12) regulates adipose tissue expansion, insulin sensitivity, and expression of inducible  
544 nitric oxide synthase. *Endocrinology*. 2014;
- 545 20. Huang G, Ge G, Wang D, Gopalakrishnan B, Butz DH, Colman RJ, et al.  $\alpha$ 3(V) Collagen is  
546 critical for glucose homeostasis in mice due to effects in pancreatic islets and peripheral tissues.  
547 *J Clin Invest*. 2011;
- 548 21. Edén D, Siegbahn A, Mokhtari D. Tissue factor/factor VIIa signalling promotes cytokine-induced  
549 beta cell death and impairs glucose-stimulated insulin secretion from human pancreatic islets.  
550 *Diabetologia*. 2015;
- 551 22. Gauger KJ, Bassa LM, Henchey EM, Wyman J, Bentley B, Brown M, et al. Mice deficient in  
552 Sfrp1 exhibit increased adiposity, dysregulated glucose metabolism, and enhanced macrophage  
553 infiltration. *PLoS One*. 2013;
- 554 23. D'souza AM, Neumann UH, Glavas MM, Kieffer TJ. The glucoregulatory actions of leptin.  
555 *Molecular Metabolism*. 2017.
- 556 24. Alcalá M, Calderon-Dominguez M, Bustos E, Ramos P, Casals N, Serra D, et al. Increased  
557 inflammation, oxidative stress and mitochondrial respiration in brown adipose tissue from obese  
558 mice. *Sci Rep*. 2017;
- 559 25. Abdullah A, Peeters A, de Courten M, Stoelwinder J. The magnitude of association between

- 560 overweight and obesity and the risk of diabetes: A meta-analysis of prospective cohort studies.  
561 Diabetes Res Clin Pract. 2010;
- 562 26. Strazzullo P, D'Elia L, Cairella G, Garbagnati F, Cappuccio FP, Scalfi L. Excess body weight and  
563 incidence of stroke: Meta-analysis of prospective studies with 2 million participants. Stroke.  
564 2010.
- 565 27. Kenchaiah S, Evans JC, Levy D, Wilson PWF, Benjamin EJ, Larson MG, et al. Obesity and the  
566 Risk of Heart Failure. N Engl J Med. 2002;
- 567 28. Rauscher GH, Mayne ST, Janerich DT. Relation between body mass index and lung cancer risk  
568 in men and women never and former smokers. Am J Epidemiol. 2000;
- 569 29. Reeves GK, Pirie K, Beral V, Green J, Spencer E, Bull D. Cancer incidence and mortality in  
570 relation to body mass index in the Million Women Study: Cohort study. Br Med J. 2007;
- 571 30. Centers for Disease Control and Prevention. National Diabetes Statistics Report. US Dep Heal  
572 Hum Serv. 2017;
- 573 31. Yang W, Dall TM, Beronjia K, Lin J, Semilla AP, Chakrabarti R, et al. Economic costs of diabetes  
574 in the U.S. in 2017. Diabetes Care. 2018;
- 575 32. Colditz GA, Willett WC, Rotnitzky A, Manson JE. Weight gain as a risk factor for clinical diabetes  
576 mellitus in women. Ann Intern Med. 1995;
- 577 33. Chatterjee S, Khunti K, Davies MJ. Type 2 diabetes. The Lancet. 2017.
- 578 34. Dulloo AG, Montani JP. Pathways from dieting to weight regain, to obesity and to the metabolic  
579 syndrome: An overview. Obesity Reviews. 2015;
- 580 35. Tomiyama AJ, Ahlstrom B, Mann T. Long-term Effects of Dieting: Is Weight Loss Related to  
581 Health? Soc Personal Psychol Compass. 2013;
- 582 36. Nathan DM, Barrett-Connor E, Crandall JP, Edelstein SL, Goldberg RB, Horton ES, et al. Long-  
583 term effects of lifestyle intervention or metformin on diabetes development and microvascular  
584 complications over 15-year follow-up: The Diabetes Prevention Program Outcomes Study.  
585 Lancet Diabetes Endocrinol. 2015;

- 586 37. MacArthur JW. Genetics of Body Size and Related Characters. I. Selecting Small and Large  
587 Races of the Laboratory Mouse. *Am Nat.* 2002;
- 588 38. Poekes L, Lanthier N, Leclercq IA. Brown adipose tissue: a potential target in the fight against  
589 obesity and the metabolic syndrome. *Clin Sci.* 2015;
- 590 39. Kajimura S, Spiegelman BM, Seale P. Cell Metabolism Review Brown and Beige Fat:  
591 Physiological Roles beyond Heat Generation. *Cell Metab.* 2015;
- 592 40. Moreno-Viedma V, Amor M, Sarabi A, Bilban M, Staffler G, Zeyda M, et al. Common  
593 dysregulated pathways in obese adipose tissue and atherosclerosis. *Cardiovasc Diabetol.* 2016;
- 594 41. Hasegawa Y, Ikeda K, Chen Y, Alba DL, Stifler D, Shinoda K, et al. Repression of Adipose  
595 Tissue Fibrosis through a PRDM16-GTF2IRD1 Complex Improves Systemic Glucose  
596 Homeostasis. *Cell Metab.* 2018;
- 597 42. Maquoi E, Munaut C, Colige A, Collen D, Roger Lijnen H. Modulation of adipose tissue  
598 expression of murine matrix metalloproteinases and their tissue inhibitors with obesity. *Diabetes.*  
599 2002;
- 600 43. Raz V, Sterrenburg E, Routledge S, Venema A, van der Sluijs BM, Trollet C, et al. Nuclear  
601 entrapment and extracellular depletion of PCOLCE is associated with muscle degeneration in  
602 oculopharyngeal muscular dystrophy. *BMC Neurol.* 2013;
- 603 44. Shu L, Chan KHK, Zhang G, Huan T, Kurt Z, Zhao Y, et al. Shared genetic regulatory networks  
604 for cardiovascular disease and type 2 diabetes in multiple populations of diverse ethnicities in the  
605 United States. *PLoS Genet.* 2017;
- 606 45. Takahashi N, Yoshizaki T, Hiranaka N, Kumano O, Suzuki T, Akanuma M, et al. The production  
607 of coagulation factor VII by adipocytes is enhanced by tumor necrosis factor- $\alpha$  or isoproterenol.  
608 *Int J Obes.* 2015;
- 609 46. Denroche HC, Kwon MM, Glavas MM, Tudurí E, Philippe M, Quong WL, et al. The role of  
610 autonomic efferents and uncoupling protein 1 in the glucose-lowering effect of leptin therapy. *Mol  
611 Metab.* 2016;

- 612 47. Nikolskiy I, Conrad DF, Chun S, Fay JC, Cheverud JM, Lawson HA. Using whole-genome  
613 sequences of the LG/J and SM/J inbred mouse strains to prioritize quantitative trait genes and  
614 nucleotides. *BMC Genomics* [Internet]. 2015 Jan [cited 2016 Jan 20];16:415. Available from:  
615 <http://www.pubmedcentral.nih.gov/articlerender.fcgi?artid=4445795&tool=pmcentrez&rendertype=abstract>  
616  
617 48. Dobin A, Davis CA, Schlesinger F, Drenkow J, Zaleski C, Jha S, et al. STAR: ultrafast universal  
618 RNA-seq aligner. *Bioinformatics* [Internet]. 2013 Jan 1 [cited 2016 Jul 27];29(1):15–21. Available  
619 from: <http://www.ncbi.nlm.nih.gov/pubmed/23104886>  
620 49. Chen Y, McCarthy D, Robinson M, Smyth GK. edgeR : differential expression analysis of digital  
621 gene expression data User's Guide. 2015.  
622 50. Zhang B, Kirov S, Snoddy J. WebGestalt: An integrated system for exploring gene sets in  
623 various biological contexts. *Nucleic Acids Res.* 2005;  
624

625 **List of Supplementary Figures:**

- 626 **Supplemental Figure 1:** Physiological parameters of the LG/J inbred mouse strain.  
627 **Supplemental Figure 2:** Brown adipose tissue quantification of LG/J mice.  
628 **Supplemental Figure 3:** SM/J adipose histology parameters and images  
629 **Supplemental Figure 4:** SM/J expression of thermogenesis related genes  
630 **Supplemental Figure 5:** SM/J thermogenic parameters  
631 **Supplemental Figure 6:** Expression patterns of key cytokine and extracellular matrix-related genes in  
632 SM/J brown and white adipose tissue  
633 **Supplemental Figure 7:** STAR alignment summaries for RNA-sequencing results

634  
635 **List of Supplementary Tables:**

- 636 **Supplemental Table 1:** High and low fat diet constituents.  
637 **Supplemental Table 2:** Differential expression results in SM/J mice.

638    **Supplemental Table 3:** Differential expression results in LG/J mice.

639

640    **RNA sequencing count data available for download at:** <http://lawsonlab.wustl.edu/data/>